

Article

The Phosphorus Adsorption and Recovery of Mg/Fe-LDHs Mulberry Rod Biochar Composite

Meina Liang^{1,2,3}, Zimeng Wu¹, Haiyan Cao¹, Kun Dong^{1,2,3,*}, Shaoyuan Bai^{1,2,3} and Dunqiu Wang^{1,2,3,*}

¹ College of Environmental Science and Engineering, Guilin University of Technology, Guilin 541006, China; liangmeina@glut.edu.cn (M.L.); wuzimeng2024@163.com (Z.W.); caohaiyan@163.com (H.C.); baisy@glut.edu.cn (S.B.)

² Guangxi Key Laboratory of Environmental Pollution Control Theory and Technology, Guilin University of Technology, Guilin 541006, China

³ Guangxi Collaborative Innovation Center for Water Pollution Control and Water Safety in Karst Area, Guilin University of Technology, Guilin 541006, China

* Correspondence: 2020005@glut.edu.cn (K.D.); wangdunqiu@sohu.com (D.W.)

Abstract: Mg/Fe layered bimetallic oxide mulberry rod biochar composites (MFBCs) were prepared from mulberry rods and characterized using electron microscopy scanning (SEM), X-ray diffraction (XRD), Fourier infrared spectroscopy (FT-IR), and X-ray photoelectron spectroscopy (XPS). We investigated the adsorption properties of MFBCs for phosphorus, which was recovered via crystallization using calcium chloride as a precipitant. According to the findings, the MFBC is a layered bimetallic oxide with a specific surface area of $70.93 \text{ m}^2 \cdot \text{g}^{-1}$. Its point of zero charge values, or pH_{zpc} , was 7.66. The removal of phosphorus using MFBCs gradually decreased with increasing pH, and the optimum pH for phosphorus removal was 4.0. The maximum phosphorus adsorption by MFBCs at 298 K was $29.682 \text{ mg} \cdot \text{g}^{-1}$ for MFBCs. The adsorption process of phosphorus onto MFBCs is a heat absorption process, and the adsorption isothermal data of phosphorus onto MFBCs fit with the Langmuir adsorption isothermal model. Phosphorus recovery is achieved when calcium chloride is added to the phosphate-enriched desorption solution at a Ca/P molar ratio of 2.2. The phosphorus product obtained from this process is very pure hydroxyphosphapatite. The recovery rate of phosphorus in the desorption solution is 99.64%.



check for updates

Citation: Liang, M.; Wu, Z.; Cao, H.; Dong, K.; Bai, S.; Wang, D. The Phosphorus Adsorption and Recovery of Mg/Fe-LDHs Mulberry Rod Biochar Composite. *Separations* **2024**, *11*, 86. <https://doi.org/10.3390/separations11030086>

Academic Editor: Qian Ping

Received: 17 February 2024

Revised: 7 March 2024

Accepted: 14 March 2024

Published: 18 March 2024



Copyright: © 2024 by the authors. Licensee MDPI, Basel, Switzerland. This article is an open access article distributed under the terms and conditions of the Creative Commons Attribution (CC BY) license (<https://creativecommons.org/licenses/by/4.0/>).

Keywords: biochar; Mg/Fe-LDHs; adsorption; phosphorus; recovery

1. Introduction

With the rapid development of industry and agriculture, the discharge of nitrogen- and phosphorus-rich domestic sewage, industrial farming wastewater and agricultural wastewater containing pesticide and chemical fertilizer residues is increasing year by year, and the excessive discharge of phosphorus-containing wastewater will have a serious impact on the environment of water bodies. The excessive discharge of phosphorus-containing wastewater will negatively affect the environment of water bodies. Research indicates that eutrophication will occur in a body of water when the total concentration of phosphorus and nitrogen in the water body exceeds $0.02 \text{ mg} \cdot \text{L}^{-1}$ and $0.2 \text{ mg} \cdot \text{L}^{-1}$, respectively [1]. Phosphorus is a non-renewable resource with a unidirectional flow characteristic in the environment, and phosphorus ore has been designated as one of the 20 minerals in our country that cannot meet the demands of the country's economic development after 2010. Economically exploitable phosphorus ore reserves may become rare or exhausted in a century [2]. As the world's population grows and phosphorus supplies become scarcer, it is becoming increasingly important from an environmental, economic, and social standpoint to create technology that will enhance phosphorus recovery and reuse [3]. Nowadays, the most widely used techniques for removing phosphorus are chemical precipitation,

biological methods, ion exchange methods, and adsorption methods [4]. Of these, the adsorption method is considered a highly effective treatment method because of its benefits, which include its low cost, no secondary pollution, and recoverable phosphate. As a result, researchers, both domestically and internationally, are focusing much of their research on this technique.

Biochar is a carbon-rich porous solid material with a wide range of properties, including high surface area, porosity, and a stable carbon matrix. It is usually prepared using a pyrolysis process under limited oxygen conditions [5]. Enhancing the affinity of biochar for anionic pollutants via modification or functionalization has emerged as a crucial approach to broadening the use of biochar technology [6]. Two-dimensional anionic clays, known as layered dimensional bimetallic hydroxides (LDHs), are composed of negatively charged equilibrium anions and positively charged metal hydroxides arranged in an interlayer [7]. Research has demonstrated that the combination of LDHs and biochar significantly improved the physicochemical properties of the resulting biochar/LDHs composites. Porous biochar, as an ideal support matrix, provides a large reaction area for the effective modification of metal hydroxides, improves adsorption capacity and adsorption rate, and prevents the aggregation of LDHs [8]. Peng et al. [9] prepared Mg/Al-LDHs composites supported by corn stover for the adsorption of phosphorus via the co-precipitation method, and the characterization results showed that the specific surface area of the material increased after modification. The highest adsorption of phosphate by this material was $286.2 \text{ mg}\cdot\text{L}^{-1}$ at pH 6, which was much higher than that of pristine biochar. The highest removal was achieved at a molar ratio of Zn/Al of 3 by calcining at 473 K, according to the results of Sidra et al.'s [10] synthesis of a series of Zn/Al-LDHs materials for phosphate adsorption at different calcination temperatures. The adsorption isotherm data were consistent with the Langmuir adsorption isotherm model.

Nowadays, the precipitation of aluminum and iron salts, hydroxycalcium phosphate crystallization (HAP), magnesium ammonium phosphate crystallization (MAP), and novel techniques represented by ion exchange are the principal techniques for recovering phosphorus from wastewater [11]. By using an acid-leaching method of incinerated sewage sludge ash (ISSA) and a phosphorus-selective adsorbent, Yu et al. [12] implemented a novel system of phosphorus recovery and demonstrated that 95% of the phosphorus could be precipitated in the desorbed solution with a calcium molar ratio of 1:3.

This study prepared Mg/Fe LDHs mulberry stem biochar composite materials and MBC mulberry stem biochar materials and characterized the two biochar materials. The structure and properties of the two materials were characterized using procedures such as X-ray diffraction (XRD), Fourier transform infrared spectroscopy (FT-IR), X-ray photoelectron spectroscopy (XPS), scanning electron microscopy (SEM), specific surface area and porosity analyzer, and Zeta potential analyzer. The chemical composition, particle size, surface morphology, and differences between the two materials were analyzed. The adsorption performance of Mg/Fe LDHs on P was studied, the effects of different adsorption factors, such as adsorption time, adsorption temperature, the initial concentration of solution, the initial pH value of the solution, etc., on the adsorption of P were investigated through the use of Mg/Fe LDHs, and the recovery rate of P when using Mg/Fe LDHs at different ratios Ca/P was investigated. The HAP crystallization method was used to recover phosphorus and achieve phosphorus cycling. Through the research of this project, new approaches can be provided for the resource utilization of agricultural waste and the improvement of phosphorus pollution in water. At the same time, it also has a promoting effect and practical significance for the widespread application of the adsorption method for phosphorus recovery.

2. Materials and Methods

2.1. Experimental Materials

The mulberry poles used in the experiment were taken from Huanjiang County, Hechi City, Guangxi Province, China. The mulberry poles were peeled, dried, crushed, passed

through a 20-mesh sieve, and placed in a desiccator for spare. Potassium dihydrogen phosphate, iron nitrate, magnesium nitrate, sodium hydroxide, sodium carbonate, and anhydrous ethanol used in the experiment were analytically pure, and the water used in the experiment was ultrapure water (prepared using the Mill-Q SP system).

2.2. Experimental Methods

The mulberry rod powder was placed in a muffle furnace and increased from room temperature to 673 K at an elevated rate of $5\text{ }^{\circ}\text{C}\cdot\text{min}^{-1}$ and charred at 673 K for 2 h to obtain mulberry rod biochar (BC). According to the Mg/Fe molar ratio of 5:1, $0.1\text{ mol}\cdot\text{L}^{-1}$ ferric nitrate and magnesium nitrate mixed solution was added to a 2 L beaker, and ultrasonic oscillation was performed with an ultrasonic oscillator at an ultrasonic frequency of 50 KHZ for 20 min. Then, 5 g of mulberry stem biochar was added, and ultrasonic oscillation was performed for another 30 min. The mixture was allowed to stand for 12 h. After being placed on a magnetic stirrer, $0.75\text{ mol}\cdot\text{L}^{-1}$ of sodium hydroxide and $0.25\text{ mol}\cdot\text{L}^{-1}$ of sodium hydroxide were added while stirring. Sodium hydroxide and $0.25\text{ mol}\cdot\text{L}^{-1}$ sodium carbonate mixed solution were added under stirring. The pH of the reaction endpoint was adjusted to 10.0. Then, the reaction endpoint was aged in a water bath at 343 K for 4 h. After cooling naturally, filtration was carried out, and the solid-phase precipitate was washed with ultrapure water several times and then washed with anhydrous ethanol when the pH of the washed filtrate was $=7.0 \pm 0.1$. Then, the solid-phase precipitate was placed on a ceramic disk and dried at 353 K for 24 h. The Mg/Fe-LDHs mulberry stick biochar (MFBCs) was ground after passing through a 100-mesh sieve, which was then placed in a desiccator and set aside.

2.3. Adsorption Experiment

In a 100 mL polyethylene centrifuge tube, $2\text{ g}\cdot\text{L}^{-1}$ of MFBCs was put into 50 mL of phosphorus-containing synthetic wastewater. The pH of the solution was adjusted with $0.1\text{ mol}\cdot\text{L}^{-1}$ NaOH and HNO_3 , and the reaction was oscillated in a thermostatic water bath oscillator at 180 rpm ($298 \pm 1\text{ K}$) until the set time, centrifuged at 4000 rpm for 5 min, and then filtered with a $0.45\text{ }\mu\text{m}$ PVDF filter membrane. The total phosphorus concentration in the filtrate was analyzed using the Ammonium molybdate spectrophotometric method. Each group of experiments contained three parallels, and the average of the experimental results was taken.

2.3.1. Effect of Solution pH on Adsorption

The initial phosphorus concentration was $20\text{ mg}\cdot\text{g}^{-1}$, and $2\text{ g}\cdot\text{L}^{-1}$ of MFBCs was put into 50 mL of phosphorus-containing synthetic wastewater with solution pH of 3, 4, 5, 6, 7, 8, 9, 10, 11, and 12, respectively. The residual phosphorus concentration was determined when the solution was shaken to adsorption equilibrium at 298 K using a thermostatic water bath oscillator. Phosphorus adsorption q_e [Equation (1)] and removal rate $R\%$ [Equation (2)] are as follows:

$$q_e = (C_0 - C_e)V/m, \quad (1)$$

$$R\% = (C_0 - C_e)/C_0, \quad (2)$$

where q_e is the amount of phosphorus adsorbed by MFBCs at the equilibrium moment, $\text{mg}\cdot\text{g}^{-1}$; C_0 is the initial phosphorus concentration in the solution, $\text{mg}\cdot\text{g}^{-1}$; C_e is the concentration of phosphorus in the solution at the time of adsorption equilibrium, $\text{mg}\cdot\text{g}^{-1}$; V is the volume of the solution, L; and m is the mass of MFBCs, g.

2.3.2. Isothermal Adsorption Experiment

The initial phosphorus concentrations were 10, 15, 20, 25, 30, 40, 50, 80, and $100\text{ mg}\cdot\text{L}^{-1}$, respectively, and the pH of the solution was adjusted to 4.0. Then, 0.1 g of MFBCs was added to 50 mL of phosphorus-containing synthetic wastewater. Additionally, the solution

was fully oscillated to equilibrium in a constant-temperature water bath oscillator at 298 K to determine the residual phosphorus concentration in the filtrate and unmodified mulberry stem biochar was used as a control. The data after adsorption equilibrium were fitted using Langmuir and Freundlich adsorption models, which were linearized in the form of [Equations (3) and (4)].

$$C_e/q_e = C_e/q_m + K_L \cdot q_m, \tag{3}$$

$$\lg q_e = \lg K_F [\lg C_e/n], \tag{4}$$

where q_e is the equilibrium adsorption amount at adsorption equilibrium, $\text{mg}\cdot\text{g}^{-1}$; C_e is the equilibrium concentration at adsorption equilibrium, $\text{mg}\cdot\text{g}^{-1}$; q_m is the maximum adsorption amount adsorbed by Langmuir's monomolecular layer; K_L and K_F are the adsorption equilibrium constants; and n is the adsorption index.

2.3.3. Adsorption Kinetics Experiment

The initial phosphorus concentrations were set at 50 and 100 $\text{mg}\cdot\text{L}^{-1}$, and 0.1 g of MFBCs was added to 50 mL of phosphorus-containing synthetic wastewater, the pH of the solution was adjusted to 4.0, and the residual phosphorus concentrations were determined at different periods of 0.25, 0.5, 1, 1.5, 3, 5, 7, 10, 12, 15, 18, 24, 36, and 48 h. The residual phosphorus concentrations were determined at different periods of 0.25, 0.5, 1, 1.5, 3, 5, 7, 10, 12, 15, 18, 24, 36, and 48 h. The residual phosphorus concentrations were determined at different times. The adsorption process was fitted using quasi-primary and quasi-secondary kinetic models with the linear expressions of [Equations (5) and (6)].

$$\text{Lg}(q_e - q_t) = \text{lg}q_e - K_1^t, \tag{5}$$

$$t/q_t = 1/K_2 \cdot q_e^2 + t/q_e, \tag{6}$$

where q_t is the adsorption of phosphorus by MFBCs at time t , $\text{mg}\cdot\text{g}^{-1}$; t is the reaction time; q_e is the equilibrium adsorption; $\text{mg}\cdot\text{g}^{-1}$; k_1 , and k_2 are the adsorption rate constants for the quasi-primary kinetic model and quasi-secondary kinetic model, respectively.

2.3.4. Adsorption Thermodynamic Experiments

The initial phosphorus concentrations were 10, 15, 20, 25, 30, 40, 50, 80, and 100 $\text{mg}\cdot\text{L}^{-1}$, and the solution pH was adjusted to 4.0. Then, 0.1 g of MFBCs was added to 50 mL of phosphorus-containing synthetic wastewater. The reaction temperatures were set at 298, 308, and 318 K, respectively, and the phosphate content in the filtrate was determined after reaching adsorption equilibrium. The thermodynamic parameters such as free energy change (ΔG), enthalpy change (ΔH), and entropy change (ΔS) were calculated by combining the Van't Hoff equation and the Gibbs–Helmholtz equation to study the adsorption thermodynamic mechanism. The Van't Hoff equation and Gibbs–Helmholtz equation are expressed as [Equations (7) and (8)].

$$\Delta G = \Delta G^0 + RT \ln Q, \tag{7}$$

$$\Delta G^0 = -RT \ln K^0 = \Delta H^0 - T \Delta S^0, \tag{8}$$

where ΔG^0 is the standard free energy change ($\text{kJ}\cdot\text{mol}^{-1}$); ΔH^0 is the standard enthalpy change ($\text{kJ}\cdot\text{mol}^{-1}$); ΔS^0 is the standard entropy change [$\text{kJ}\cdot(\text{mol}\cdot\text{K})^{-1}$]; Q is the reaction quotient; R is the standard gas constant [$R = 8.3145 \text{ J}\cdot(\text{K}\cdot\text{mol})^{-1}$]; and K^0 is the standard equilibrium constant.

2.4. Phosphorus Recovery Experiment

The saturated MFBCs adsorbed in the phosphate solution with an initial phosphorus concentration of 100 $\text{mg}\cdot\text{L}^{-1}$ were desorbed with 0.1 $\text{mg}\cdot\text{L}^{-1}$ NaOH solution, and the pH

of the desorbed solution was adjusted to be about 10. Anhydrous calcium chloride with Ca/P molar ratios of 1.67, 2.0, 2.2, 2.5, and 3.0 was added to the desorbed solution, and the desorbed solution was placed in a magnetic stirrer with stirring for 1 h. The solution was allowed to stand for 30 min and then centrifuged. The solid phase precipitate was placed in a 353 K drying oven for 12 h, ground, and stored in a desiccator. The phosphorus recovery rate R_2 is calculated by the following Equation (9):

$$R_2 = (C_0 - C_1)/C_0 \times 100, \tag{9}$$

where C_0 is the concentration of phosphorus in the desorption solution, $\text{mg}\cdot\text{L}^{-1}$, and C_1 is the concentration of phosphorus contained in the desorption solution after phosphorus recovery, $\text{mg}\cdot\text{L}^{-1}$.

3. Results and Discussion

3.1. Characterization of MFBCs

3.1.1. Specific Surface Area Analysis

Figure 1 shows the nitrogen adsorption–desorption isotherms and pore size distribution of MFBCs and MBC. According to the Brunauer–Emmet–Teller theory, MFBCs exhibit type IV isotherms in the relative pressure range of 0.1–0.9, indicating that MFBCs are mesoporous [13]. The results showed that the adsorption capacity of MFBCs and MBC gradually increased with the increase in relative pressure, and the adsorption/desorption curve of the MBC in the low-pressure region (0.15–0.40 relative pressure (P/P^0)) showed a significant increase, indicating that MBC contains more abundant mesoporous and microporous structures than MFBCs [14].

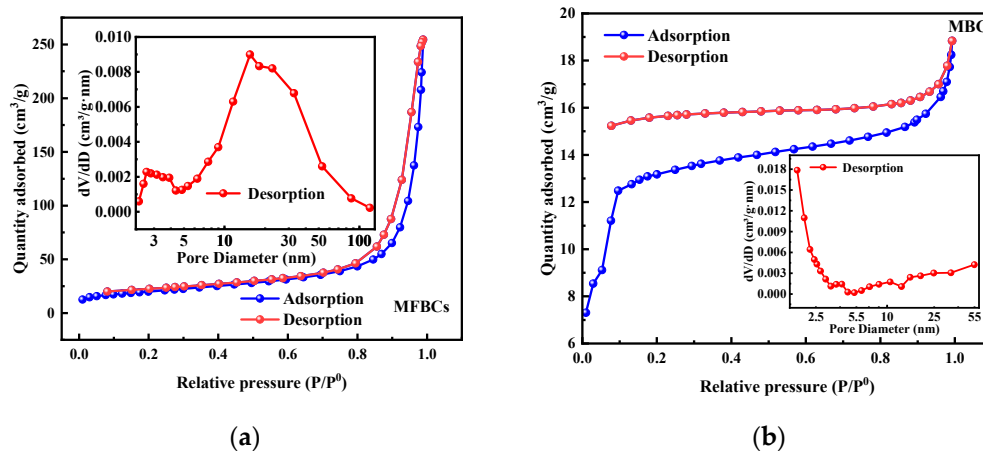


Figure 1. N_2 adsorption/desorption isotherms and pore size distribution: (a) MFBCs; (b) BC.

The results of the specific surface area and pore size analysis of BC and MFBCs are shown in Table 1. The table shows that the specific surface areas of BC and MFBCs were $51.91 \text{ m}^2\cdot\text{g}^{-1}$ and $70.93 \text{ m}^2\cdot\text{g}^{-1}$, respectively. Compared with BC, the specific surface area of MFBCs increased, the total pore volume increased, and a larger pore size was obtained, which belonged to the mesopore range ($2 \text{ nm} < d < 50 \text{ nm}$), and the mesopore structure of the surface was favorable to the adsorption process, leading to the increased heterogeneity of MFBCs, which can provide more adsorption sites for phosphate [15]. On the other hand, after modification by Mg and Fe, the surface functional groups of MFBCs were activated, the content of surface-active groups increased, hydrophilicity was strengthened, and the adsorption capacity for phosphorus was enhanced [16].

Table 1. Specific surface area and aperture analysis of BC and MFBCs.

Material	Specific Surface Area /m ² ·g ⁻¹	Average Pore Diameter /nm	Total Pore Volume /cm ³ ·g ⁻¹
BC	51.91	2.2449	0.029
MFBCs	70.93	22.1980	0.394

3.1.2. Zeta Analysis

Figure 2 shows the zeta potential versus pH curves for BC and MFBCs. From Figure 1, the zeta potentials (pH_{ZPC}) of BC and MFBCs were 2.35 and 7.66, respectively, which shows that the zeta potential of the modified MFBCs was significantly increased compared to BC, indicating that MFBCs has a more significant surface hydroxyl density and protonated hydroxyls present a stable positive charge over a wide pH range and will enhance phosphate adsorption by electrostatic attraction [17].

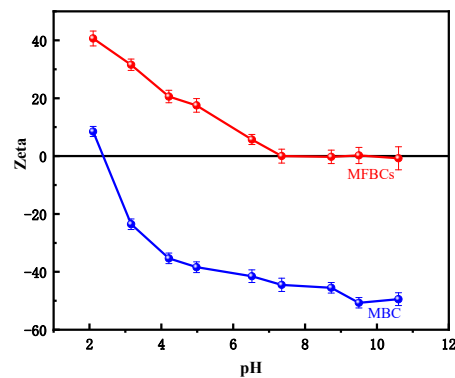
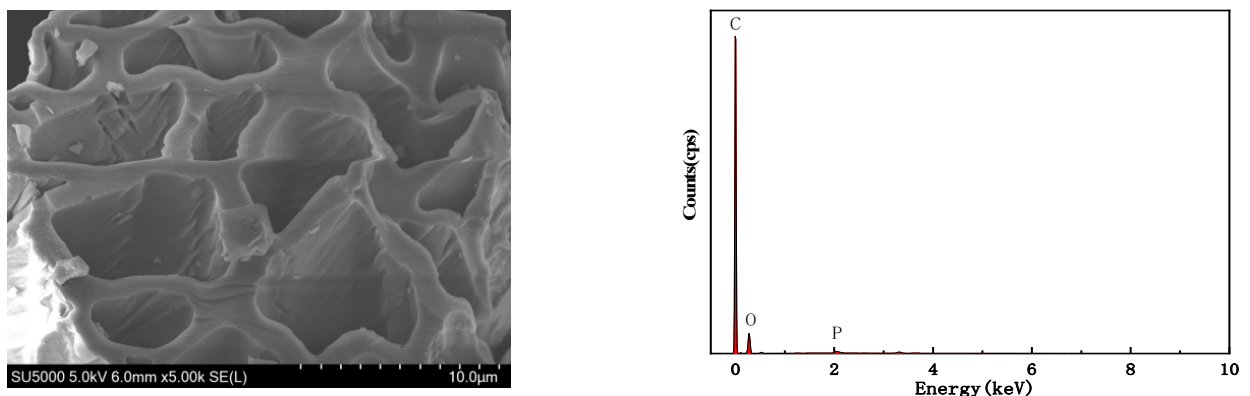


Figure 2. Zeta potential and pH values for BC and MFBCs.

3.1.3. SEM Analysis

The SEM and EDS characterization results of BC and MFBCs are displayed in Figure 2. From Figure 3a, it can be seen that the surface and inner wall of BC are smooth with a prominent pore structure, which mainly consists of C and O elements and contains a small amount of P. From Figure 3b, it can be seen that the surface and the inner part of the pores of MFBCs are covered with metal oxides, which improves the specific surface area, increasing the active sites and the chance of binding with pollutants. Prominent peaks of Fe and Mg elements appeared in the EDS energy spectrum, and the elemental distribution map (c) showed that Fe and Mg were uniformly dispersed in MFBCs, indicating that Fe and Mg were successfully loaded on the mulberry stick biochar.



(a)

Figure 3. Cont.

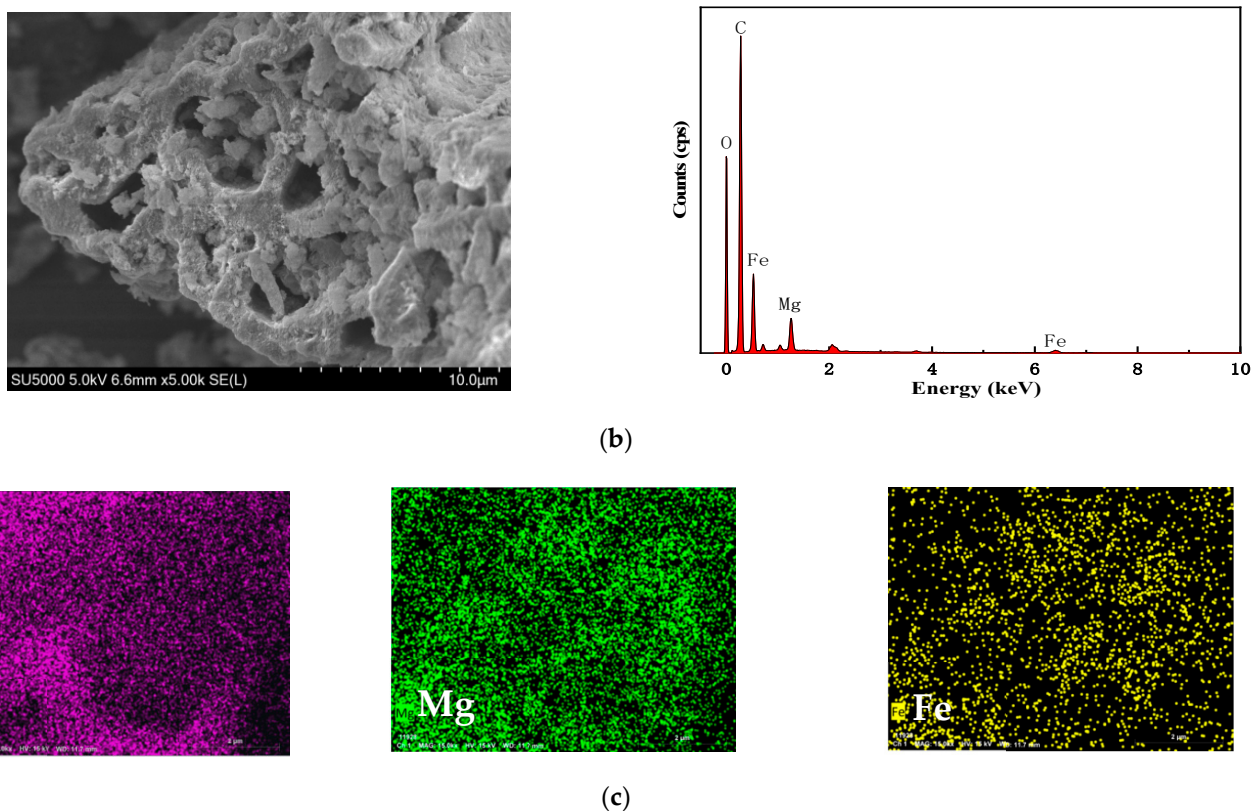


Figure 3. SEM and EDS plots and element distribution plots: (a) BC; (b) MFBCs; (c) MFBCs.

3.1.4. FT-IR Analysis

The results of the FT-IR analysis of BC and MFBCs are shown in Figure 4. From Figure 4, it can be seen that BC and MFBCs have characteristic peaks at 3449 cm^{-1} , 1629 cm^{-1} and 3446 cm^{-1} , 1620 cm^{-1} , respectively. According to the corresponding profiles of infrared functional groups, it can be seen that the broad bands at 3446 cm^{-1} and 3449 cm^{-1} indicated that the occurrence of water molecules and O-H bonding in the upper layer and the Mg-Fe/LDH intercalation layer was caused by the stretching-type vibrations of the groups [18]. There are C=O stretching vibration peaks at $1680\text{--}1630\text{ cm}^{-1}$; the peak at 1620 cm^{-1} is related to the bending mode of the water molecules in the interlayer, and the peak of MFBCs at 1368 cm^{-1} suggests the presence of the asymmetric stretching of the carbonate molecules in the layer [19]. In addition, the characteristic peaks at 587 cm^{-1} indicated the presence of the asymmetric stretching of carbonate molecules associated with the mixed-metal oxide (Fe-O or Mg-O or MgFe-O)-related adsorption bands [20], thus indicating the successful synthesis of Mg/Fe-LDHs.

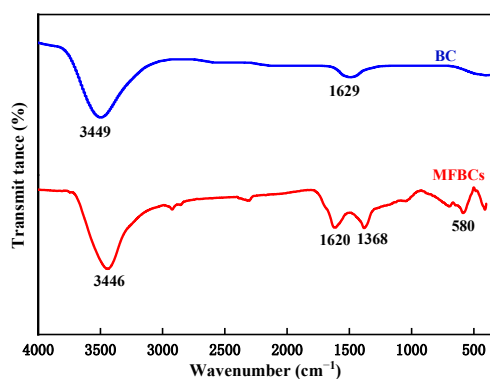


Figure 4. FT-IR profiles of BC and MFBCs.

3.1.5. XRD Analysis

Figure 5 shows the XRD patterns of BC and MFBCs. Compared with BC, MFBCs have the characteristic diffraction peaks of Mg/Fe-LDHs, including the typical planes of (003), (006), (012), and (018), which proved the formation of the LDH phase, indicating that the Mg/Fe-LDHs were synthesized efficiently and loaded on mulberry stem biochar successfully.

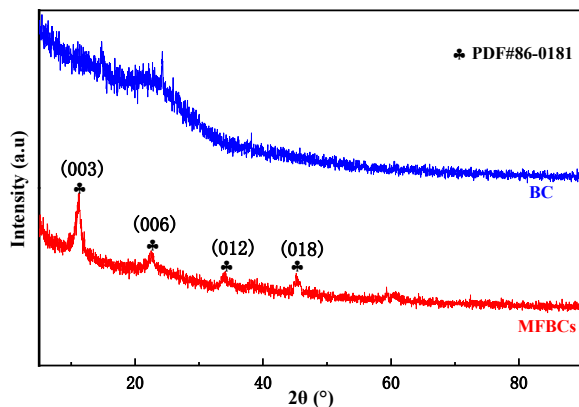


Figure 5. The XRD profiles of BC and MFBCs.

3.1.6. XPS Analysis

Figure 6 shows the XPS images of BC and MFBCs; as can be seen in Figure 6a, the BC surface is mainly composed of C and O elements, and the MFBCs surface has Mg and Fe elements in addition to C and O. There is no obvious change in the binding energy positions of C 1s and O 1s. Still, the peak at O 1s is significantly enhanced, indicating that the content of metal (hydro)oxides or oxygen-containing functional groups has increased due to the modification [21]. MFBCs show peaks at 700.18–739.98 eV for Fe 2p and 1296.18–1308.98 eV for Mg 1s. From Figure 6b, the peaks of C 1s in MFBCs appeared at 284.8 eV, 286.5 eV, and 288.6 eV for C-C, C-O, and O-C=O, respectively. According to Figure 6d, the Mg 1s spectrum is mainly Mg-O-Fe (1303.33–1303.81 eV), indicating that magnesium in MFBCs exists in oxide form. Figure 6c shows that the position of the Fe 2p 3/2 characteristic peak is at 711.49 eV, and its sub-peak contains the characteristic peak of trivalent iron of Fe₂O₃ (712.58 eV).

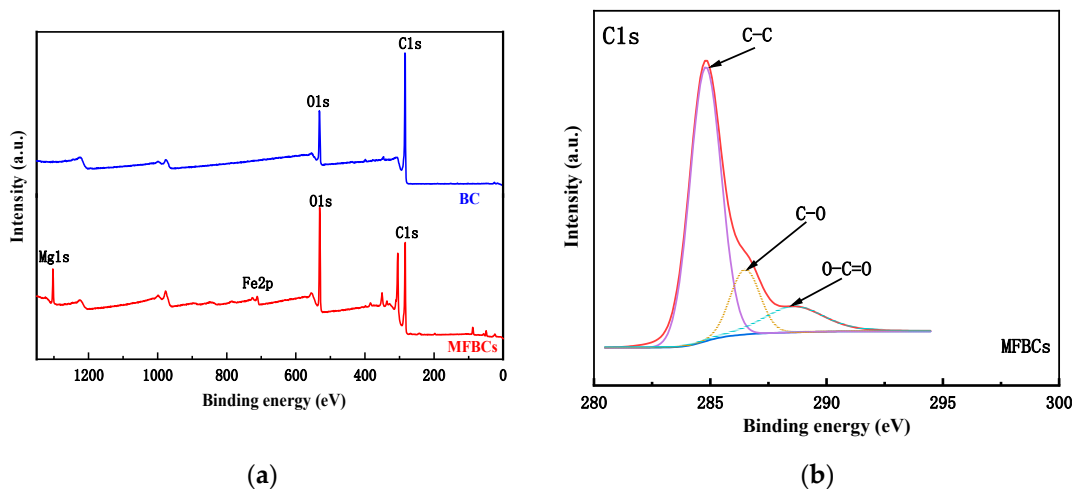


Figure 6. Cont.

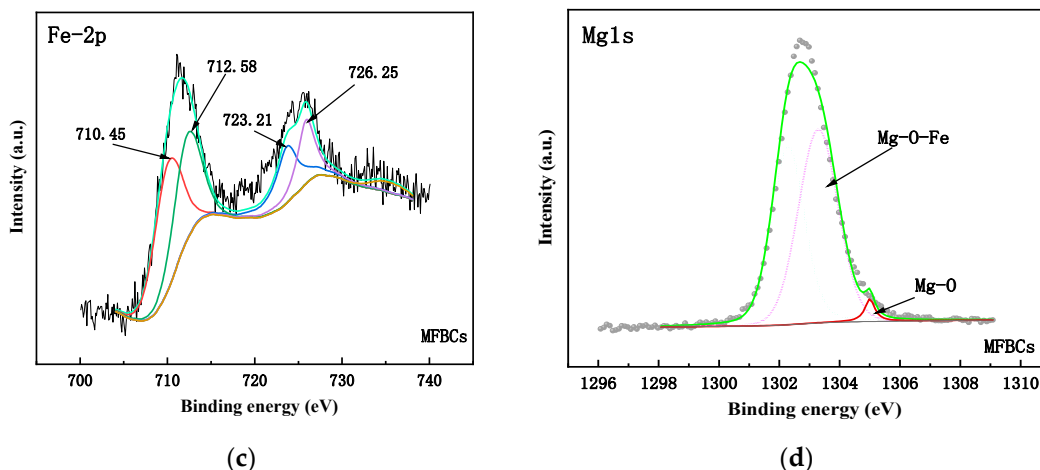


Figure 6. XPS plots for BC and MFBCs (a) Full XPS spectrum scan; (b) C 1s of MFBCs; (c) Fe 2p of MFBCs; (d) Mg 1s of MFBCs.

3.2. Effect of Solution pH on Adsorption

The effect of pH on phosphorus adsorption by MFBCs is shown in Figure 7. As can be seen in Figure 7, the removal of phosphorus was more significant than 90% when the solution pH was <6. When the pH is between 3 and 4, the phosphorus removal rate increases with the increase in pH. When pH = 4, the removal rate and adsorption capacity of phosphorus are both highest, at 99.33% and 29.682 mg·g⁻¹, respectively. When the pH is between 4 and 6, the phosphorus removal rate decreases by 1.89% as the pH increases. Phosphorus removal gradually decreased in the pH 6~12 range and was below 50% when the solution pH was greater than 8.0. The reason for this phenomenon may be because pH can affect the ionization equilibrium of phosphate, and different pH presents different phosphate forms; when the pH is in the range of 2.12–7.20, the main phosphate form in the solution is H₂PO₄⁻, when the pH is in the range of 7.20–12.36, the main phosphate form in the solution is HPO₄²⁻, and when the pH is above 12.36, the major phosphate form in the solution is PO₄³⁻ [22]. From 3.1.6, the pH_{pc} of MFBCs = 7.66. When pH < pH_{zpc}, the adsorbent surface is protonated, mostly positively charged, and there is an electrostatic attraction with negatively charged PO₄³⁻P. The phosphate removal mechanism is mainly electrostatic attraction and ligand exchange, which results in a larger removal rate of phosphorus; when pH > pH_{zpc}, the electrostatic repulsion between the negatively charged surface sites and the phosphate ion. The electrostatic repulsion between the negatively charged surface sites and phosphate ions increases, and at this time, the ligand exchange is the main adsorption mechanism. With the rise in pH, the OH⁻ concentration in the solution increases. The phosphate root produces competitive adsorption, and the removal rate of phosphorus decreases [23].

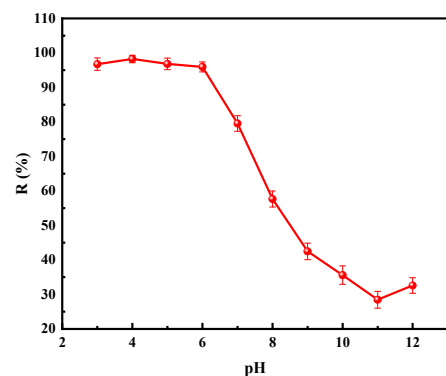


Figure 7. Effect of solution pH on MFBCs.

3.3. Isothermal Adsorption Lines

The adsorption isotherms of phosphorus by MFBCs at 298, 308, and 318 K, respectively, are shown in Figure 8. The results showed that the adsorption amount decreased slightly with increasing temperature. The maximum adsorption amount was $29.682 \text{ mg}\cdot\text{g}^{-1}$, $29.121 \text{ mg}\cdot\text{g}^{-1}$, and $28.417 \text{ mg}\cdot\text{g}^{-1}$ at 298, 308, and 318 K, respectively. With the increase in the initial phosphorus concentration, phosphate adsorption significantly increased and then gradually reached equilibrium. The decrease in phosphate adsorption can be explained by the lack of active sites capable of accommodating the increased phosphate species at immobilized adsorbent doses [24]. The significant increase in phosphorus adsorption after modification compared to unmodified mulberry stem biochar suggested that the combination of porous biochar matrix and positively charged Mg/Fe-LDHs has a strong enhancement effect on anion adsorption.

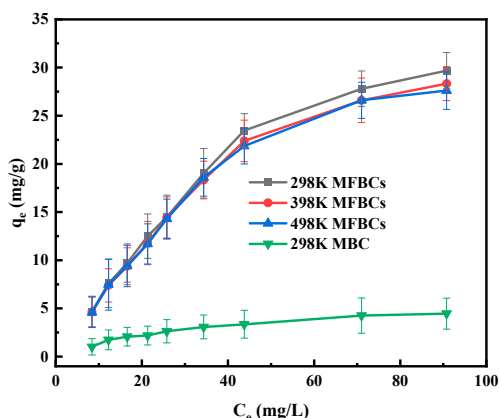


Figure 8. Adsorption isotherm of phosphorus by MFBCs.

The Langmuir and Freundlich adsorption isothermal model was applied to fit this curve, and the results are shown in Figure 9. Based on the slope and intercept of the fitted straight line, the relevant parameters of the two models at 298, 308, and 318 K can be obtained, respectively, as shown in Table 2.

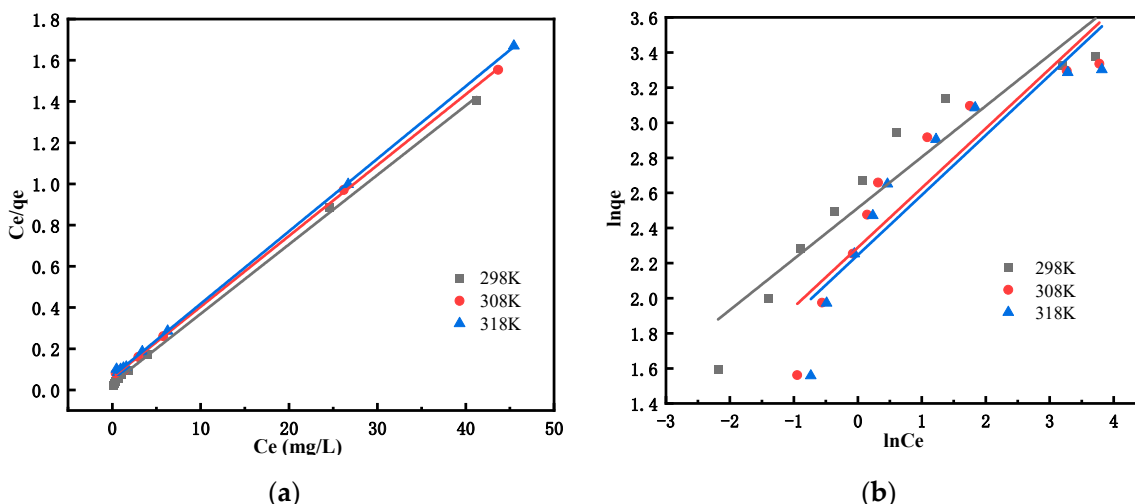


Figure 9. Fitting of Langmuir and Freundlich models for MFBC adsorption of phosphorus. (a) Langmuir model; (b) Freundlich model.

Table 2. Langmuir and Freundlich isothermal parameters for the phosphorus adsorption on MFBCs at different temperatures.

T/K	$q_{exp}/mg \cdot g^{-1}$	Langmuir Equation			Freundlich Equation		
		$q_{cal}/mg \cdot g^{-1}$	b	R^2	K	1/n	R^2
298	29.311	29.682	0.0324	0.9994	12.354	0.2906	0.8875
308	28.097	29.121	0.0605	0.9998	9.864	0.3392	0.8289
318	27.207	28.417	0.0660	0.9998	9.449	0.3413	0.8209

Figure 9 and Table 2 show that the Langmuir adsorption isothermal model fits the adsorption process better. The correlation coefficients R^2 of the fitted straight line are 0.9994, 0.9998, and 0.9998, respectively, which are larger than those of the Freundlich adsorption isothermal model when the temperatures are 298, 308, and 318 K. The theoretical maximum adsorption amount q_{cal} calculated from the Langmuir adsorption isothermal model is closer to the actual maximum adsorption amount q_{exp} , indicating that the maximum adsorption amount is 29.682 $mg \cdot g^{-1}$. The theoretical maximum adsorption amount q_{cal} calculated using the Langmuir adsorption isothermal model was closer to the actual maximum adsorption amount q_{exp} . The maximum adsorption amount was 29.682 $mg \cdot g^{-1}$, which indicated that the Langmuir adsorption isothermal model was able to better describe the adsorption process of phosphorus, which was dominated by chemical adsorption. The effective adsorption surface showed the characteristics of a monolayer of homogeneity [25]. The maximum adsorption amount of phosphorus by MFBCs was approximately the same as that of the adsorption isothermal model by Jia [26] et al. The adsorption was about 5.3 times higher than the maximum adsorption of phosphorus by Mg-Al-Fe layered double hydroxides prepared by Jia et al. (5.61 $mg \cdot g^{-1}$); they were 3.0 and 1.2 times higher than the maximum adsorption of phosphorus by Mg-Al and Zn-Al layered double hydroxides (LDHs) synthesized by Yang [27] et al. (9.78 and 24.8 $mg \cdot g^{-1}$); they were 1.4 and 2.4 times the maximum adsorption of phosphorus by Ce/Fe₃O₄-BC and La/Fe₃O₄-BC new rare earth-doped magnetic biochar prepared by Wang [28] et al. (20.5 and 12.5 $mg \cdot g^{-1}$); and the maximum adsorption of phosphorus by the MFBCs prepared in the present study was more significant. The adsorption of the Freundlich isotherm modeling strength and nonuniformity parameters (i.e., 1/n) ranged from 0 to 1, indicating that phosphate was readily adsorbed on MFBCs.

3.4. Adsorption Kinetic Modeling

The adsorption kinetic curve of MFBCs on phosphorus is shown in Figure 10. With the increase in reaction time, the adsorption amount first increased rapidly and then increased slowly until the adsorption equilibrium was reached, which was because as the reaction proceeded, the adsorption sites on the adsorbent surface available for binding gradually reduced, and the rate of mass transfer was slowed down until the binding sites were all occupied and the reaction reached equilibrium. The adsorption reaction reached equilibrium at about 5 h when the initial phosphorus concentration was 50 $mg \cdot g^{-1}$, and the adsorption equilibrium time was prolonged and reached equilibrium at about 20 h when the initial phosphorus concentration increased to 100 $mg \cdot g^{-1}$.

To further investigate the adsorption process of phosphorus by MFBCs, a pseudo-first-order-kinetic model and a pseudo-second-order kinetic model were applied to fit the adsorption process. The results are shown in Figure 11. The kinetic parameters of the two models were obtained based on the slopes and the intercepts of the fitted straight lines, shown in Table 3.

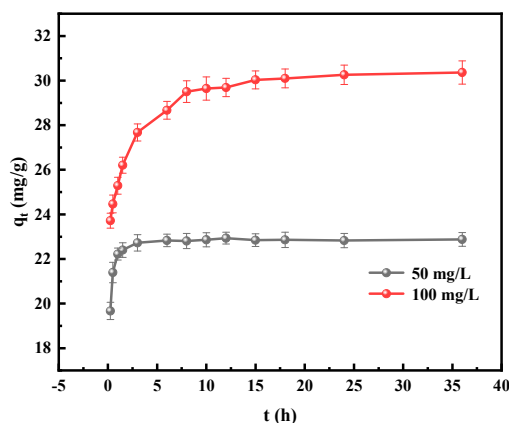


Figure 10. Kinetic curves of P adsorption in MFBCs.

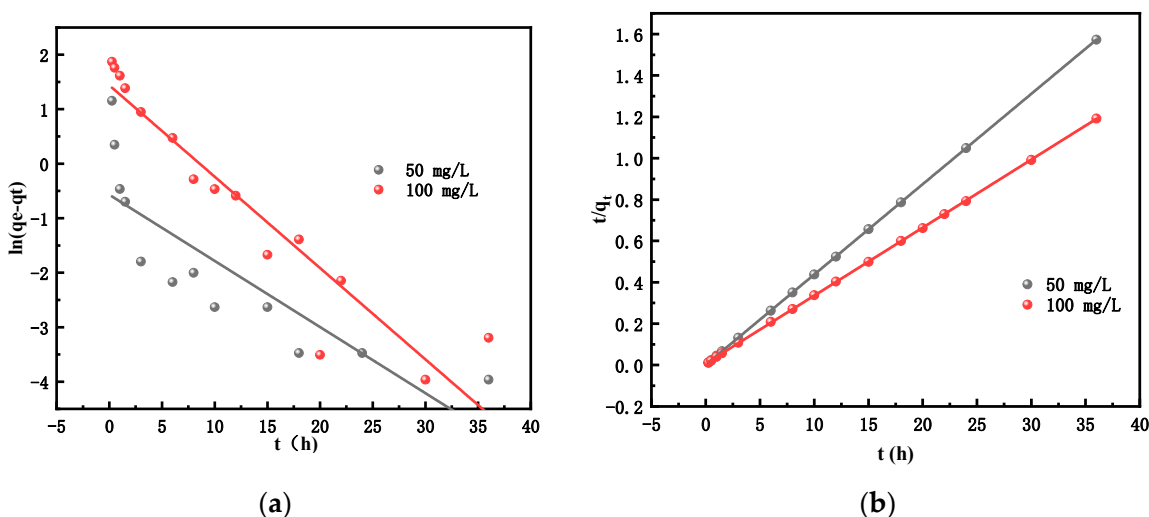


Figure 11. Fitting of pseudo-first-order-kinetic model and pseudo-second-order kinetic model for MFBCs adsorption of phosphorus. (a) pseudo-first-order-kinetic model; (b) pseudo-second-order kinetic model.

Table 3. Dynamic parameters of phosphorus adsorption by MFBCs.

Initial Phosphorus Concentration /mg·g ⁻¹	q _{exp} /mg·g ⁻¹	Pseudo-First-Order-Kinetics			Pseudo-Second-Order Kinetics		
		q _{cal} /mg·g ⁻¹	K ₁	R ²	q _{cal} /mg·g ⁻¹	K ₂	R ²
50	22.906	1.300	0.1213	0.6855	22.96	1.009	1
100	30.254	4.21	0.1676	0.8863	30.43	0.151	0.999

As can be seen from Figure 11 and Table 3, the correlation coefficients R² of the pseudo-first-order-kinetic model fit were 0.6855 and 0.8863 when the initial phosphorus concentrations were 50 and 100 mg·L⁻¹, respectively, and the correlation coefficients R² of the pseudo-second-order kinetic model fit were 1 and 0.999, respectively, which clearly showed that the pseudo-first-order-kinetic model had a better fitting effect. In addition, the theoretical adsorption amount q_{cal} calculated by the pseudo-second-order kinetic model fitting was closer to the actual adsorption amount q_{exp}. From this, it can be hypothesized that the adsorption process of phosphorus by MFBCs is mainly chemisorption, and there may be electron exchange or sharing during the adsorption process [29]. The phosphorus in the solution diffuses to the surface of MFBCs and forms new compounds immobilized on its surface active sites through chemical bonding or ion exchange.

3.5. Adsorption Thermodynamic Parameters

As shown in Figure 8, the adsorption of phosphorus by MFBCs decreased with increasing temperature, indicating that low temperature favors the adsorption of phosphorus by MFBCs. To further investigate the spontaneity and stability of phosphorus adsorption by MFBCs, each thermodynamic parameter at 298, 308, and 318 K was found according to Equations (7) and (8), respectively, and are listed in Table 4. As seen in Table 4, the standard free energy change of adsorption of phosphorus by MFBCs at 298.15 K, $\Delta G^0 = -0.094 \text{ kJ}\cdot\text{mol}^{-1} < 0$, indicates that the phosphorus adsorption by MFBCs is spontaneous. The adsorption of phosphorus by MFBCs is a spontaneous process, and increasing the temperature weakens the spontaneity of adsorption. The absolute value of ΔG^0 increases with increasing temperature, indicating that the driving force of the adsorption process increases. The enthalpy change of phosphorus adsorption by MFBCs, $\Delta H^0 = -26.104 \text{ kJ}\cdot\text{mol}^{-1} < 0$, indicates that the adsorption process is an exothermic reaction process, and the entropy change, $\Delta S^0 = -0.088 \text{ kJ}\cdot\text{mol}^{-1}\cdot\text{K}^{-1} < 0$, indicates that the adsorption process is an exothermic reaction process. As the adsorption reaction proceeds, the entropy of the system decreases, and the orderliness increases [30]. Since the absolute value of ΔH^0 for physical adsorption is generally in the range of 0–20 $\text{kJ}\cdot\text{mol}^{-1}$, the absolute value of ΔH^0 for chemical adsorption is greater than 20 $\text{kJ}\cdot\text{mol}^{-1}$, indicating that the adsorption of phosphorus by MFBCs is mainly chemical adsorption [31].

Table 4. Thermodynamic parameters of the adsorption system.

T/K	$K_L/\text{L}\cdot\text{mg}^{-1}$	$\Delta G^0/\text{KJ}\cdot\text{mol}^{-1}$	$\Delta S^0/\text{KJ}\cdot(\text{mol}\cdot\text{K})^{-1}$	$\Delta H^0/\text{KJ}\cdot\text{mol}^{-1}$
298	1.039	−0.094		
308	0.567	1.453	−0.088	−26.104
318	0.533	1.665		

3.6. Phosphorus Recovery Studies

3.6.1. Effect of Calcium–Phosphorus Ratio on Phosphorus Recovery

The effect of different calcium–phosphorus ratios on phosphorus recovery is shown in Figure 12. It can be seen that as the calcium–phosphorus ratio increases, the phosphorus concentration in the desorbent decreases, and the phosphorus recovery R_2 increases. When the calcium–phosphorus ratio increased from 1.67 to 2.2, the phosphorus concentration C_1 in the desorbent decreased rapidly from $3.104 \text{ mg}\cdot\text{L}^{-1}$ to $0.194 \text{ mg}\cdot\text{L}^{-1}$, and the phosphorus recovery R_2 increased from 94.45% to 99.64%, which was basically able to completely recover the phosphorus in the desorbent, and continued to increase the calcium–phosphorus ratio, the phosphorus concentration and the recovery did not change significantly.

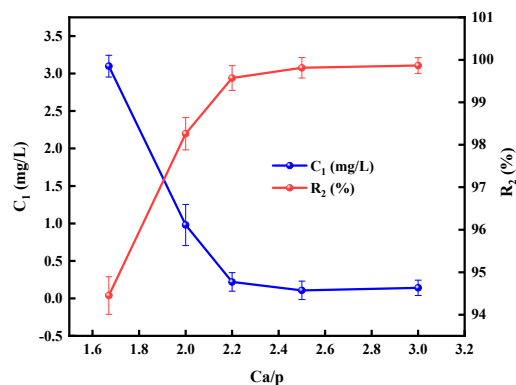


Figure 12. Effect of different calcium/phosphorus ratios on phosphorus recovery.

When $\text{Ca}/\text{P} = 2.2$, the recovery rate of phosphorus is 99.64%. The recovery rate of phosphorus by MFBCs is about 1.06 times that of the maximum recovery rate of phosphorus (94%) when using the Mg- Al- Fe layered double hydroxides prepared by Jia et al. [24].

Xiong et al. [21] synthesized a novel aqueous phosphorus removal adsorbent by simultaneously loading zirconia and iron oxide onto activated carbon nanofibers (ACF-ZrFe), achieving a maximum phosphorus recovery rate of 1.08 times (91.4%). It is 1.02 times and 2.4 times the maximum phosphorus adsorption capacity (97.9%) of La(OH)₃-modified bentonite prepared by Huang et al. [20]. Therefore, the MFBCs prepared in this study have a higher maximum recovery rate for phosphorus.

Under the influence of Ca/P and pH, the reactants may preferentially generate precursors such as amorphous calcium phosphate (ACP), dicalcium phosphate (DCP), tricalcium phosphate (TCP), octacalcium phosphate (OCP), etc. These precursors are then further converted into hydroxyapatite HAP. When pH = 10 and Ca/P = 2.2, Ca²⁺, OH⁻, and phosphate ions can directly form HAP. When Ca/P < 2.2, the reactants will first form amorphous precursors and then generate HAP, and some amorphous precursors cannot be converted. When the Ca/P molar ratio is greater than 2.2, it may be due to the presence of CaCO₃, which increases the composition of Ca²⁺. CaCO₃ replaces the crystallization sites of HAP, and the reactants form amorphous precursors such as ACP, DCP, TCP, OCP, etc. [32].

3.6.2. Characterization of Recovered Phosphorus Products

The recovered phosphate was a white powder, and in order to analyze its crystal structure and major functional groups, it was analyzed via XRD and FT-IR, and the results are shown in Figure 13.

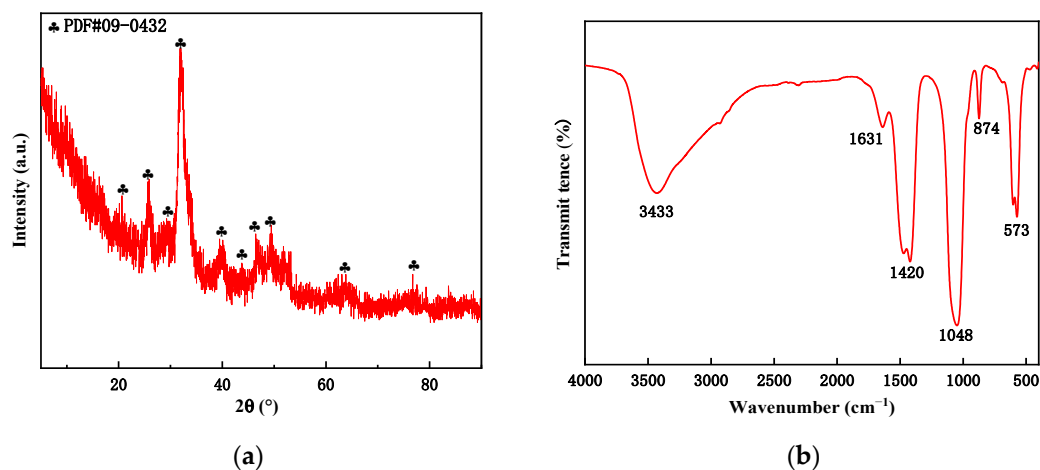


Figure 13. XRD (a) and FT-IR (b) profiles of recovered phosphorus products.

The XRD pattern of the recycled phosphorus product is shown in Figure 13a, with strong diffraction peaks at $2\theta = 26^\circ, 33^\circ, 34^\circ, 35^\circ,$ and 40° , which are basically the same as the position of the peaks of the standard hydroxyapatite PDF card (JCPDF 09-0432). Because of the lack of sintering, the diffraction peak lines are not sharp enough. The degree of crystallization is not high. However, no miscellaneous peaks, such as calcium phosphate and calcium hydroxide, indicated that the recycled product was hydroxyapatite with high purity.

The FT-IR spectrum of the recovered phosphorus product is shown in Figure 13b, which indicates that there is a telescopic vibrational absorption peak of OH⁻ at 3433 cm^{-1} , and the ν_3 vibrational peaks of PO₄³⁻ in hydroxyapatite appeared at $1010\text{--}1110\text{ cm}^{-1}$, while the ν_4 and ν_1 vibrational peaks of PO₄³⁻ in hydroxyapatite appeared at $560\text{--}610\text{ cm}^{-1}$. The absorption peaks generated by the splitting of the ν_3 telescopic vibration peak of CO₃²⁻ appeared near 1420 cm^{-1} , and ν_2 was located at 874 cm^{-1} , all of which are the characteristic peaks of hydroxyapatite [33,34]. In addition, the presence of the C=C telescopic vibration at 1631 cm^{-1} [35] further suggests that the recovered phosphorus, whose main constituent is hydroxyapatite, is a more desirable recycled product.

In summary, it can be seen that the recovered phosphorus product is high-purity hydroxyapatite, and the main components are C, Ca, O, H, and P, all of which are environ-

mentally friendly elements that plants and animals can directly absorb and, therefore, can be directly added to the soil as a high-value-added fertilizer while having the dual role of increasing the phosphorus content of the soil and improving the physical properties of the soil, and this strategy can also achieve the recycling of phosphorus and the virtuous cycle in the ecosystem [36].

4. Conclusions

Mulberry rods from agricultural waste were combined with layered bimetallic oxides to create MFBCs, an effective phosphorus removal adsorbent. According to characterization studies, MFBCs are layered bimetallic oxides with a zero-point potential (pH_{zpc}) of 7.66 and a specific surface area of $70.93 \text{ m}^2 \cdot \text{g}^{-1}$.

The maximum phosphorus adsorption at 298 K was $29.682 \text{ m}^2 \cdot \text{g}^{-1}$, which is greater than the maximum phosphorus adsorption by comparable materials. MFBCs have a high phosphorus removal rate in the pH range of 3–6. Phosphorus is adsorbed by an exothermic mechanism consistent with the pseudo-second-order kinetic model and the Langmuir adsorption isothermal model.

When the Ca/P ratio is 2.2, the phosphorus recovery rate R_2 reaches 99.64% using the calcium hydroxy phosphate precipitation technique, which is more effective in recovering phosphorus from the desorption solution. The recovered phosphorus product's SEM, XRD, and FT-IR analysis revealed that it was high-purity hydroxyapatite. This more desired recovered product may be used as phosphorus fertilizer.

Author Contributions: Conceptualization, Z.W. and M.L.; Methodology, M.L. and H.C.; Formal analysis, Z.W., K.D. and H.C.; Investigation, K.D., M.L., D.W. and S.B.; Resources, K.D. and D.W.; Data curation, H.C., M.L. and Z.W.; Writing—original draft, H.C., Z.W. and M.L.; Writing—review and editing, K.D., S.B. and M.L.; Visualization, Z.W., M.L. and K.D.; Supervision, D.W., M.L. and K.D.; Project administration, D.W.; Funding acquisition, M.L., K.D. and D.W. All authors have read and agreed to the published version of the manuscript.

Funding: This research was funded by the National Natural Science Foundation of China (grant number 52260024), the Guangxi key research and development plan projects (AB22080067) and the Research funds of The Guangxi Key Laboratory of Theory and Technology for Environmental Pollution Control (guikeneng 2301Z003).

Data Availability Statement: The data that support the findings of this study are available from the corresponding author upon reasonable request.

Conflicts of Interest: The authors declare no conflicts of interest.

References

1. De-Bashan, L.E.; Bashan, Y. Recent advances in removing phosphorus from wastewater and its future use as fertilizer. *Water Res.* **2004**, *38*, 4222–4246. [[PubMed](#)]
2. Cordell, D.; Drangert, J.O.; White, S. The story of phosphorus: Global food security and food for thought. *Glob. Environ. Chang.* **2009**, *19*, 292–305.
3. Melia, P.M.; Cundy, A.B.; Sohi, S.P.; Hooda, P.S.; Busquets, R. Trends in the recovery of phosphorus in bioavailable forms from wastewater. *Chemosphere* **2017**, *186*, 381–395.
4. Xing, C.; Wen, J.; Li, W.; Shi, J.; Wang, S.; Xu, Z. Integrating the $\text{Fe}^{2+}/\text{H}_2\text{O}_2^-$ strengite method in airlift reactor for phosphorus removal and recovery from organic phosphorus wastewater. *Chem. Eng. J.* **2023**, *475*, 146093.
5. Ahmad, M.; Rajapaksha, A.U.; Lim, J.E.; Zhang, M.; Bolan, N.; Mohan, D.; Vithanage, M.; Lee, S.S.; Ok, Y.S. Biochar as a sorbent for contaminant management in soil and water: A review. *Chemosphere* **2014**, *99*, 19–33.
6. Chen, B.; Chen, Z.; Lv, S. A novel magnetic biochar efficiently sorbs organic pollutants and phosphate. *Bioresour. Technol.* **2011**, *102*, 716–723. [[CrossRef](#)] [[PubMed](#)]
7. Li, Y.; Gao, B.; Wu, T.; Sun, D.; Li, X.; Wang, B.; Lu, F. Hexavalent chromium removal from aqueous solution by adsorption on aluminum magnesium mixed hydroxide. *Water Res.* **2009**, *43*, 3067–3075. [[CrossRef](#)] [[PubMed](#)]
8. He, H.; Zhang, N.; Chen, N.; Lei, Z.; Shimizu, K.; Zhang, Z. Efficient phosphate removal from wastewater by MgAl-LDHs modified hydrochar derived from tobacco stalk. *Bioresour. Technol. Rep.* **2019**, *8*, 100348.
9. Peng, Y.; Sun, Y.; Hanif, A.; Shang, J.; Shen, Z.; Hou, D.; Zhou, Y.; Chen, Q.; Ok, Y.S.; Tsang, D.C. Design and fabrication of exfoliated Mg/Al layered double hydroxides on biochar support. *J. Clean. Prod.* **2021**, *289*, 125142.

10. Iftekhar, S.; Küçük, M.E.; Srivastava, V.; Repo, E.; Sillanpää, M. Application of zinc-aluminium layered double hydroxides for adsorptive removal of phosphate and sulfate: Equilibrium, kinetic and thermodynamic. *Chemosphere* **2018**, *209*, 470–479. [[PubMed](#)]
11. Lin, H.; Wang, Y.; Dong, Y. A review of methods, influencing factors and mechanisms for phosphorus recovery from sewage and sludge from municipal wastewater treatment plants. *J. Environ. Chem. Eng.* **2023**, *12*, 111657.
12. Yu, X.; Nakamura, Y.; Otsuka, M.; Omori, D.; Haruta, S. Development of a novel phosphorus recovery system using incinerated sewage sludge ash (ISSA) and phosphorus-selective adsorbent. *Waste Manag.* **2020**, *120*, 41–49. [[CrossRef](#)] [[PubMed](#)]
13. Ding, C.; Long, X.; Zeng, G.; Ouyang, Y.; Lei, B.; Zeng, R.; Wang, J.; Zhou, Z. Efficiency Recycling and Utilization of Phosphate from Wastewater Using LDHs-Modified Biochar. *Int. J. Environ. Res. Public Health* **2023**, *20*, 3051. [[PubMed](#)]
14. Guo, H.; Liu, Y.; Lv, Y.; Liu, Y.; Lin, Y.; Liu, M. Nitrogen doped sinocalamus oldhami lignin-based activated biochar with high specific surface area: Preparation and its adsorption for malachite green contaminant. *Process Saf. Environ. Prot.* **2024**, *183*, 992–1001. [[CrossRef](#)]
15. Fan, Y.A.; Sz, A.; Ys, B.; Tsang, D.C.; Cheng, K.; Ok, Y.S. Assembling biochar with various layered double hydroxides for enhancement of phosphorus recovery—ScienceDirect. *J. Hazard. Mater.* **2019**, *365*, 665–673.
16. Wu, L.; Xu, D.; Li, B.; Wu, D.; Yang, H. Enhanced removal efficiency of nitrogen and phosphorus from swine wastewater using MgO modified pig manure biochar. *J. Environ. Chem. Eng.* **2024**, *12*, 111793.
17. Liao, T.; Li, T.; Su, X.; Song, H.; Zhu, Y.; Zhang, Y. La(OH)₃-modified magnetic pineapple biochar as novel adsorbents for efficient phosphate removal. *Bioresour. Technol.* **2018**, *263*, 207–213. [[CrossRef](#)] [[PubMed](#)]
18. Zubair, M.; Daud, M.; McKay, G.; Shehzad, F.; Al-Harathi, M.A. Recent progress in layered double hydroxides (LDH)-containing hybrids as adsorbents for water remediation. *Appl. Clay Sci.* **2017**, *143*, 279–292.
19. Yang, Y.; Tan, X.; Almatrafi, E.; Ye, S.; Song, B.; Chen, Q.; Tan, X.; Yang, H.; Fu, Q.; Deng, Y.; et al. Alfalfa biochar supported Mg-Fe layered double hydroxide as filter media to remove trace metal (loid) s from stormwater. *Sci. Total Environ.* **2022**, *844*, 156835. [[CrossRef](#)] [[PubMed](#)]
20. Alagha, O.; Manzar, M.; Zubair, M.; Anil, I.; Mu'azu, N.D.; Qureshi, A. Magnetic Mg-Fe/LDH Intercalated Activated Carbon Composites for Nitrate and Phosphate Removal from Wastewater: Insight into Behavior and Mechanisms. *Nanomaterials* **2020**, *10*, 1361. [[CrossRef](#)]
21. Wang, Y.; Li, J.; Xu, L.; Wu, D.; Li, Q.; Ai, Y.; Liu, W.; Li, D.; Zhang, B.; Guo, N.; et al. EDTA functionalized Mg/Al hydroxides modified biochar for Pb (II) and Cd (II) removal: Adsorption performance and mechanism. *Sep. Purif. Technol.* **2023**, *333*, 126199. [[CrossRef](#)]
22. Huang, W.; Li, D.; Liu, Z.Q.; Tao, Q.; Zhu, Y.; Yang, J.; Zhang, Y.M. Kinetics, isotherm, thermodynamic, and adsorption mechanism studies of La(OH)₃-modified exfoliated vermiculites as highly efficient phosphate adsorbents. *Chem. Eng. J.* **2014**, *236*, 191–201.
23. Triantafyllidis, K.S.; Peleka, E.N.; Komvokis, V.G.; Mavros, P.P. Iron-modified hydrotalcite-like materials as highly efficient phosphate sorbents. *J. Colloid Interface Sci.* **2010**, *342*, 427–436. [[CrossRef](#)]
24. Wu, X.; Zhan, R.; Liu, L.; Lan, J.; Zhao, N.; Wang, Z. Phosphorus Adsorption on Blast Furnace Slag with Different Magnetism and Its Potential for Phosphorus Recovery. *Water* **2022**, *14*, 2452. [[CrossRef](#)]
25. Benyoucef, S.; Amrani, M. Adsorption of phosphate ions onto low cost Aleppo pine adsorbent. *Desalination* **2011**, *275*, 231–236.
26. Jia, Z.; Hao, S.; Lu, X. Exfoliated Mg-Al-Fe layered double hydroxides/polyether sulfone mixed matrix membranes for adsorption of phosphate and fluoride from aqueous solutions. *J. Environ. Sci.* **2017**, *70*, 63–73. [[CrossRef](#)]
27. Yang, K.; Yan, L.G.; Yang, Y.M.; Yu, S.J.; Shan, R.R.; Yu, H.Q.; Zhu, B.C.; Du, B. Adsorptive removal of phosphate by Mg–Al and Zn–Al layered double hydroxides: Kinetics, isotherms and mechanisms. *Sep. Purif. Technol.* **2014**, *124*, 36–42.
28. Wang, L.; Wang, J.; He, C.; Lyu, W.; Zhang, W.; Yan, W.; Yang, L. Development of rare earth element doped magnetic biochars with enhanced phosphate adsorption performance. *Colloids Surf. A Physicochem. Eng. Asp.* **2019**, *561*, 236–243.
29. Xiao, J.; Hu, R.; Chen, G.; Xing, B. Facile synthesis of multifunctional bone biochar composites decorated with Fe/Mn oxide micro-nanoparticles: Physicochemical properties, heavy metals sorption behavior and mechanism. *J. Hazard. Mater.* **2020**, *399*, 123067. [[PubMed](#)]
30. Kılıç, M.; Yazıcı, H.; Solak, M. A comprehensive study on removal and recovery of copper (II) from aqueous solutions by NaOH-pretreated *Marrubium globosum* ssp. *globosum* leaves powder: Potential for utilizing the copper (II) condensed desorption solutions in agricultural applications. *Bioresour. Technol.* **2009**, *100*, 2130–2137. [[CrossRef](#)]
31. Kim, T.H.; Lundehj, L.; Nielsen, U.G. An investigation of the phosphate removal mechanism by MgFe layered double hydroxides. *Appl. Clay Sci.* **2020**, *189*, 105521.
32. Blanco, I.; Molle, P.; de Miera, L.E.; Ansoła, G. Basic oxygen furnace steel slag aggregates for phosphorus treatment. Evaluation of its potential use as a substrate in constructed wetlands. *Water Res.* **2016**, *89*, 355–365. [[CrossRef](#)] [[PubMed](#)]
33. Ng, S.; Guo, J.; Ma, J.; Loo, S.C.J. Synthesis of high surface area mesostructured calcium phosphate particles. *Acta Biomater.* **2010**, *6*, 3772–3781. [[CrossRef](#)]
34. Wang, F.; Li, M.S.; Lu, Y.P.; Qi, Y.X.; Liu, Y.X. Synthesis and microstructure of hydroxyapatite nanofibers synthesized at 37 °C. *Mater. Chem. Phys.* **2006**, *95*, 145–149. [[CrossRef](#)]

35. Liu, G.; Zhang, X.; Liu, H.; He, Z.; Show, P.L.; Vasseghian, Y.; Wang, C. Biochar/layered double hydroxides composites as catalysts for treatment of organic wastewater by advanced oxidation processes: A review. *Environ. Res.* **2023**, *234*, 116534. [[PubMed](#)]
36. Manoukian, L.; Metson, G.S.; Hernández, E.M.; Vaneckhaute, C.; Frigon, D.; Omelon, S. Forging a cohesive path: Integrating life cycle assessments of primary-origin phosphorus fertilizer production and secondary-origin recovery from municipal wastewater. *Resour. Conserv. Recycl.* **2023**, *199*, 107260.

Disclaimer/Publisher's Note: The statements, opinions and data contained in all publications are solely those of the individual author(s) and contributor(s) and not of MDPI and/or the editor(s). MDPI and/or the editor(s) disclaim responsibility for any injury to people or property resulting from any ideas, methods, instructions or products referred to in the content.